

## Synthesis of biodegradable polycaprolactone/ polyurethane by curing with H<sub>2</sub>O

Chi-Hui Tsou<sup>1,2</sup> · Hsun-Tsing Lee<sup>3</sup> ·  
Manuel De Guzman<sup>2</sup> · Hui-An Tsai<sup>4</sup> ·  
Pin-Ning Wang<sup>4</sup> · Hsiang-Jung Cheng<sup>5</sup> ·  
Maw-Cherng Suen<sup>4</sup>

Received: 27 August 2014 / Revised: 2 February 2015 / Accepted: 3 March 2015 /  
Published online: 20 March 2015  
© Springer-Verlag Berlin Heidelberg 2015

**Abstract** To prepare a pre-polymer in this study, the following materials were used: 4,4'-diphenylmethane diisocyanate, poly( $\epsilon$ -caprolactone) diol (PCL), and polytetramethylene ether glycol. The pre-polymer was then cured using H<sub>2</sub>O to form a new type of polyurethane (PU), PCL/H<sub>2</sub>O-PU. Fourier transform infrared analysis confirmed the successful synthesis of PCL/H<sub>2</sub>O-PU. Results from thermal gravimetric analysis, differential scanning calorimetry, and dynamic mechanical analysis showed that the thermal resistance and glass transition temperature of PCL/H<sub>2</sub>O-PU increased with the H<sub>2</sub>O and the hard segment content. Stress–strain curves for the PCL/H<sub>2</sub>O-PU specimens showed that with increasing H<sub>2</sub>O content, the tensile strength and Young's modulus increased, but the elongation at break decreased. WAXD patterns indicated that with a higher H<sub>2</sub>O content, the polymer chains were in a more ordered arrangement, although the morphology was still amorphous. The degree of swelling in an aqueous ethanol solution and the hydrolytic degradation rate increased with the PCL content. Scanning electron microscopic images showed that during the degradation period, the original wrinkled

---

✉ Maw-Cherng Suen  
sun@tiit.edu.tw

<sup>1</sup> Department of Materials Science and Engineering, National Taiwan University of Science and Technology, Taipei 10607, Taiwan, ROC

<sup>2</sup> Department of Chemical Engineering, R&D Center for Membrane Technology, Chung Yuan University, Jhongli, Taoyuan 32023, Taiwan, ROC

<sup>3</sup> Nanomaterials Applications R&D Center, Vanung University, Jongli, Taoyuan 32091, Taiwan, ROC

<sup>4</sup> Department of Creative Fashion Design, Taoyuan Innovation Institute of Technology, Jongli, Taoyuan 32091, Taiwan, ROC

<sup>5</sup> Graduate School of Materials Applied Technology, Taoyuan Innovation Institute of Technology, Jongli, Taoyuan 32091, Taiwan, ROC

surface of PCL/H<sub>2</sub>O-PU became smooth, and then cracks were formed. The cracks became more severe when the degradation was at a higher temperature.

**Keywords** Biodegradable · Polycaprolactone diol · Hydrolytic degradation · Polyurethane

## Introduction

In the polyurethane (PU) industry, curing with moisture is a type of water-based technology. One-component PU-urea systems have several advantages: hardness, abrasion resistance, thermal stability, solvent and chemical resistance, and high humidity tolerance. These properties are related to the degree of curing [1, 2]. On the basis of differential scanning calorimetry and dynamic mechanical analysis, Chattopadhyay et al. [3, 4] reported on the change in the sample short-range enthalpy order and stability with the curing time. The degree of phase mixing after a certain period depends on the soft segment structure and stability. Nomura et al. [5] showed that silane end cappers could be used to synthesize a PU end capped with trimethoxysilane without purification, which could be employed as a base polymer for moisture-curable, one-component solvent-free elastic adhesives. Ren et al. [6] showed two models about curing with moisture, which employed a symmetric diisocyanate that gave rise to a soft continuous phase; the commercially relevant adhesive was prepared from a less symmetric polyisocyanate that produced a hard continuous phase. Other new environment-friendly PUs were obtained by glycolysis of a waste PU [7–10] or halogen-free flame retardants [11]. Those new materials show good mechanical properties and performance.

Biodegradable polymers are more and more widely used as long-lasting polymers for short-lived applications. A lot of research has reported the improvement in the properties, [12, 13] biodegradation [12], and biocompatibility [14] of their polymer composites. Biodegradable PUs have biological compatibility and excellent physical properties, so they have been substantially used in the medical or environmental industries [15]. They are typically synthesized with soft segments susceptible to hydrolysis, such as poly(alkylene adipate), poly( $\epsilon$ -caprolactone) (PCL), poly(lactide), and poly(glycolide) [16–23]. Segmented PU elastomers have been used as biomaterials for several decades because of their unique physicochemical properties and favorable biocompatibility [24]. PCL is used as a resorbable soft segment diol, and desamino tyrosyl-tyrosine hexyl ester is used as a degradable hard segment chain extender [25–28]. In our recent study, 2,6-pyridinedimethanol (2,6-PDM) was used as a chain extender to prepare a biodegradable PU [29] or an antibacterial PU [30]. The results showed that the thermal resistance, glass transition temperature, tensile strength, and elongation at break of the biodegradable PU increased with the 2,6-PDM content. In this study, the synthesis was performed by curing with moisture; soft- and hard segment ratios were varied. A study on the hydrolytic degradation and the thermal resistance of potential PU could be important in predicting the biodegradability and the chemical and physical characteristics of a new type of PU.



**Table 1** Data on the different compounds of PCL/H<sub>2</sub>O-PU

Compound	MDI (mole)	PTMG (mole)	PCL (mole)	H <sub>2</sub> O (mole)	Hard segment (wt%)	Soft segment (wt%)	Swelling degree (%)
PCL/H <sub>2</sub> O-PU-01	4	2	1	1	28.69	71.31	47.7 ± 0.4
PCL/H <sub>2</sub> O-PU-02	4	2	0.8	1.2	29.65	70.35	46.8 ± 0.2
PCL/H <sub>2</sub> O-PU-03	4	2	0.5	1.5	31.21	68.79	46.6 ± 0.2
PCL/H <sub>2</sub> O-PU-04	4	2	0.3	1.7	32.31	67.69	45.9 ± 0.1

circulating oven at 70 °C for 3 h. The resulting films were cooled and stripped from the dish by immersing them in distilled water for several hours. After drying them at 70 °C for several hours, smooth and free-standing PCL/H<sub>2</sub>O-PU films were finally obtained. Each specimen was analyzed with FTIR-ATR to confirm that the prepolymer NCO group at wavenumbers 2275 and 2240 cm<sup>-1</sup> fully disappeared. The mechanism for the reaction between H<sub>2</sub>O and prepolymer is as follows:

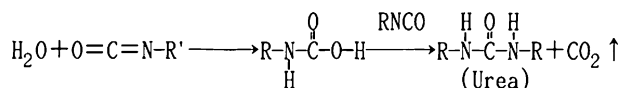


Table 1 shows the formula that represents each compound of PCL/H<sub>2</sub>O-PU, the amount of constituents, and the properties of the compound. The hard segment content was calculated using Eq. (2.1). Equation (2.2) shows the calculation of the soft-segment content.

$$\text{Hard-segment content (wt\%)} = \frac{W_{\text{MDI}} + W_{\text{H}_2\text{O}}}{W_{\text{MDI}} + W_{\text{PTMG}} + W_{\text{PCL}} + W_{\text{H}_2\text{O}}} \times 100 \%, \quad (2.1)$$

$$\text{Soft-segment content (wt\%)} = 100 - \text{hard-segment content} \quad (2.2)$$

where  $W_{\text{MDI}}$  is the weight of MDI,  $W_{\text{H}_2\text{O}}$  is the weight of H<sub>2</sub>O, and  $W_{\text{PCL}}$  is the weight of PCL.

### Fourier transform infrared (FT-IR) spectroscopy

FTIR measurements were performed on a Perkin Elmer spectrometer (model Spectrum One). Each sample spectrum was obtained by averaging 15 scans in a wavenumber range of 4000 to 650 cm<sup>-1</sup> and with a resolution of 2 cm<sup>-1</sup>.

### Thermogravimetric analysis (TGA)

A Perkin Elmer TGA (model Pyris 1) was used. Samples (8–10 mg) were heated from room temperature to 700 °C under nitrogen at a rate of 10 °C/min.

### Differential scanning calorimetry (DSC)

A Perkin Elmer DSC (model Jade) was used. Samples were sealed in aluminum pans; they were scanned (−100 to 300 °C) at a heating rate of 10 °C/min under nitrogen purging. DSC thermograms were taken from the first run. The glass transition temperature, based on the maximum peak of the endothermic transition in the second scan, was recorded. Samples of approximately 7–8 mg were used for all tests.

### Dynamic mechanical analysis (DMA)

A TA DMA (model Q800) was run at 1 Hz with a 5- $\mu$ m amplitude over a temperature range of −80 to 100 °C and at a heating rate of 3 °C/min; it was conducted with a tension mode. A specimen measured 20  $\times$  5  $\times$  0.2 mm (L  $\times$  W  $\times$  T). The glass transition temperature was taken as the peak temperature of the glass transition region in the tan  $\delta$  curve.

### Stress–strain testing

Tensile strength and elongation at break were measured using a universal testing machine (model QTest 5). Testing was conducted with ASTM D638. A specimen film had a dimension of 45  $\times$  8  $\times$  0.2 mm (L  $\times$  W  $\times$  T).

### Gel permeation chromatography (GPC)

A gel permeation chromatography (model 500, Analytical Scientific Instruments), with a reflection index (RI) detector (Schambeck RI2000) and two columns in a series of Jordi gel DVB mixed bed and 10,000 Å bed at 30 °C, was used to measure the molecular weight distribution relative to polystyrene standards. The calibration curve was obtained on the basis of eight standards from molecular weights 3420 to  $2.57 \times 10^6$ . The carrier solvent was tetrahydrofuran at a flow rate of 1 ml/min.

### Swelling degree

A specimen film with a dimension of 3  $\times$  3 cm was dried to a constant weight ( $W_d$  = weight of dried film) in a circulating oven at 120 °C for 24 h. Subsequently, the dried specimen was placed in a sealed conical flask containing 100 ml of 20 wt% aqueous ethanol solution for 24 h. The swollen specimen was then taken out of the flask, wiped with a filter paper, and weighed ( $W_w$  = weight of swollen film). The swelling degree was calculated according to Eq. (2.3):

$$\text{Swelling degree} = \frac{W_w - W_d}{W_d} \times 100 \%. \quad (2.3)$$

## Wide angle X-ray diffraction (WAXD)

WAXD was measured using a Rigaku diffractometer (model RU-H3R). The X-ray beam operated on a Ni-filtered  $\text{CuK}\alpha$  radiation from a sealed tube at 60 kV and 300 mA. Data were obtained in the  $2\theta$  range of  $2^\circ$ – $40^\circ$  with a scanning interval of  $0.05^\circ$ .

## Hydrolytic degradation tests

The hydrolytic degradation evaluation of a specimen was conducted in a 3 % aqueous NaOH solution at 37 and 45 °C. The specimen with dimensions of  $2 \times 2 \text{ cm}^2$  was tested for several days, washed with distilled water, and dried completely in a vacuum oven at 70 °C for 3 h. The degree of degradation was determined from the weight loss calculated with Eq. (2.4):

$$\text{Weight loss} = \frac{W_0 - W_t}{W_0} \times 100 \%, \quad (2.4)$$

where  $W_0$  is the dry weight before degradation, and  $W_t$  is the dry weight at time  $t$ .

## Morphology analysis

The specimen morphology before and after the hydrolytic degradation was observed by using a Hitachi scanning electron microscope (SEM) (model SU1510). Specimens of  $2 \times 2 \text{ cm}^2$  were fixed on a sample holder with a conductive double-sided adhesive tape and were then coated with a thin layer of gold to improve the image resolution. The samples were photographed at 3.00 K magnification.

## Results and discussion

### Chemical structure

The FT-IR spectra of the PCL/ $\text{H}_2\text{O}$ -PU compounds in Fig. 1 indicate four common main peaks at these wavenumbers: 2939, 2856, 1729, and  $1220 \text{ cm}^{-1}$ . The first two peaks refer to the stretching vibration of the alkyl C–H group; the third peak refers to the stretching vibration of C=O; the fourth to the C–O stretching vibration. Other characteristic peaks in the spectra of PCL-MDI and PCL/ $\text{H}_2\text{O}$ -PU compounds are 3333 to  $3287 \text{ cm}^{-1}$ , which is due to the N–H stretching absorption;  $1535 \text{ cm}^{-1}$ , the C=C stretching vibration; and  $816 \text{ cm}^{-1}$ , the –CH bending vibration. The last two peaks are also observed in the spectrum of PCL. The appearance of a peak at  $1532 \text{ cm}^{-1}$ , corresponding to the CHN vibration of associated secondary urethane groups, proves the success of synthesizing PCL/MDI by the urethanization reaction. The spectrum of PCL/MDI has a unique peak at 2278 to  $2250 \text{ cm}^{-1}$ , which is associated with the unreacted –N=C=O groups. These groups would react with the

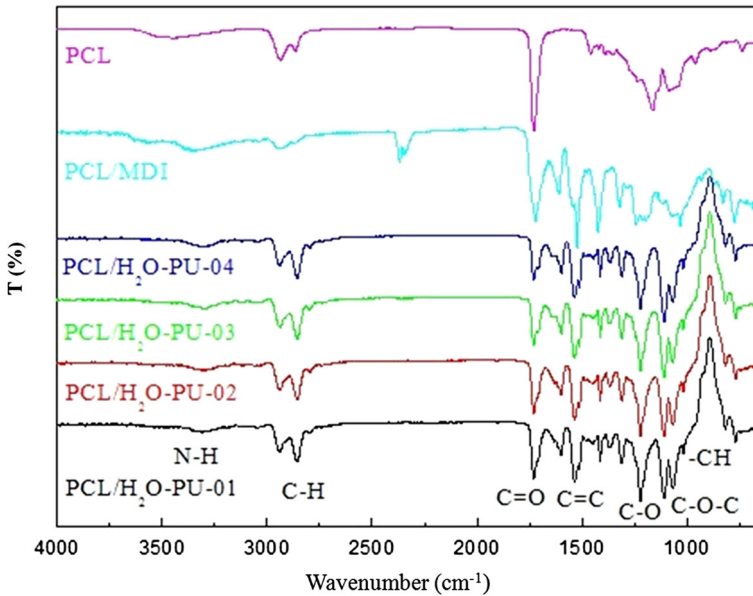


**Fig. 1** FTIR spectra of PCL, PCL/MDI and PCL/H<sub>2</sub>O-PU

–OH groups of H<sub>2</sub>O in the subsequent step to form PCL/H<sub>2</sub>O-PU. The absence of the –N=C=O stretching vibration peak in the spectra of PCL/H<sub>2</sub>O-PU indicates that the reaction did occur to successfully synthesize the compound.

### Thermal properties

Figure 2 shows the TGA and differential thermogravimetric (DTG) curves of different compounds of PCL/H<sub>2</sub>O-PU; Table 2 tabulates their thermal properties. The onset decomposition temperature ( $T_{\text{onset}}$ ) for PCL/H<sub>2</sub>O-PU-01, PCL/H<sub>2</sub>O-PU-02, PCL/H<sub>2</sub>O-PU-03, and PCL/H<sub>2</sub>O-PU-04 is 329, 330, 332, and 333 °C, respectively. The decomposition temperature peak ( $T_{\text{max}}$ ) for these compounds is at 409, 414, 416, and 419 °C, respectively. Of the four compounds, PCL/H<sub>2</sub>O-PU-01 contains the lowest H<sub>2</sub>O content, whereas PCL/H<sub>2</sub>O-PU-04 has the highest. The hard-segment content increases with the H<sub>2</sub>O content. Therefore, the decomposition temperature or the thermal resistance increases with the H<sub>2</sub>O or the hard-segment content. Moreover, the higher residual of PCL/H<sub>2</sub>O-PU-01 after the degradation (>500 °C) might be because of the better thermostability of the soft-segment with the highest content at high temperature. A similar phenomenon has been reported in our previous study [29].

Figure 3 presents the DSC thermograms of PCL/H<sub>2</sub>O-PU. From DSC, the glass transition temperature ( $T_g$ ) of PCL/H<sub>2</sub>O-PU-01, PCL/H<sub>2</sub>O-PU-02, PCL/H<sub>2</sub>O-PU-03, and PCL/H<sub>2</sub>O-PU-04 is –43, –41, –40, and –39 °C, respectively. This increasing trend is similar to that of the aforementioned decomposition temperature.

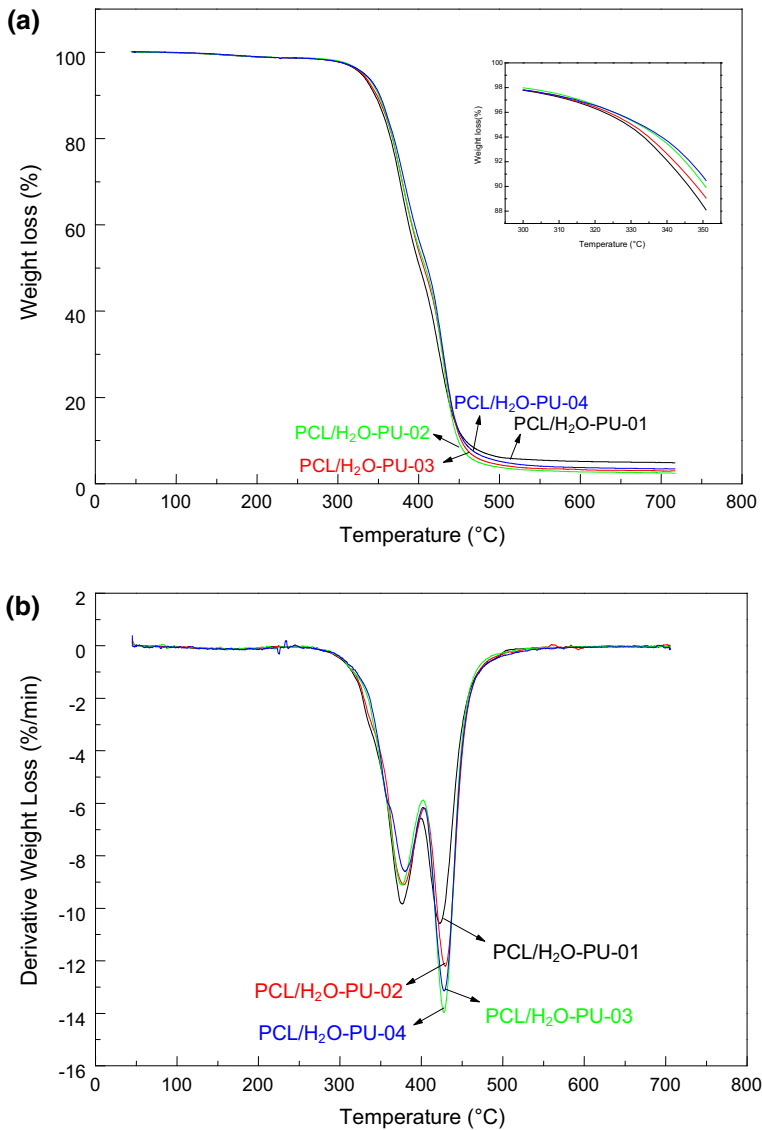


**Fig. 2** a TGA and b DTG curves of PCL/H<sub>2</sub>O-PU

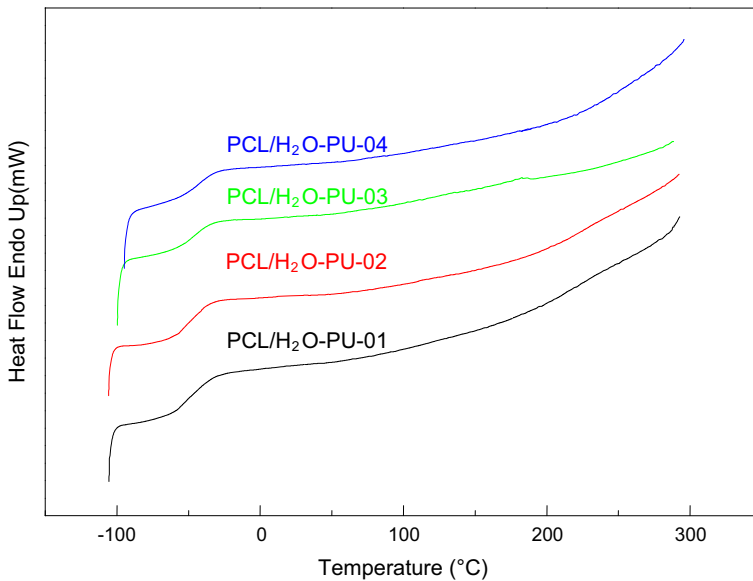
Decreasing the PCL or the soft-segment content results in a high decomposition temperature of PU, whereas increasing the H<sub>2</sub>O or the hard-segment content enhances the thermostability.

### Dynamic mechanical properties

Figure 4a–c shows the change in loss modulus, storage modulus, and loss factors with the H<sub>2</sub>O content, respectively. Dynamic mechanical spectral curves change

**Table 2** Thermal properties of PCL/H<sub>2</sub>O-PU

Compound	TGA		DSC	DMA
	$T_{\text{onset}}$ (°C)	$T_{\text{max}}$ (°C)	$T_g$ (°C)	$T_g$ (°C)
PCL/H <sub>2</sub> O-PU-01	328.9 ± 0.3	409.2 ± 0.2	-43.3 ± 0.4	-35.1 ± 0.3
PCL/H <sub>2</sub> O-PU-02	329.5 ± 0.1	414.1 ± 0.4	-41.2 ± 0.2	-33.7 ± 0.2
PCL/H <sub>2</sub> O-PU-03	331.8 ± 0.2	415.7 ± 0.3	-40.1 ± 0.3	-30 ± 0.1
PCL/H <sub>2</sub> O-PU-04	332.9 ± 0.4	418.8 ± 0.5	-39.3 ± 0.2	-29 ± 0.2

**Fig. 3** DSC thermograms of PCL/H<sub>2</sub>O-PU

with each compound composition. The decrease in values of storage modulus with the H<sub>2</sub>O content at 25 °C indicates that PCL/H<sub>2</sub>O-PU is less elastic with increasing hard-segment content (Table 2). The results can be attributed to the denser structure associated with the presence of moisture for curing purposes.

Figure 4c illustrates the dependence of  $\tan \delta$  on temperature. The transition peak in the range of -35.1 to -29 °C can be assigned as the dynamic  $T_g$  of PCL/H<sub>2</sub>O-PU. Moreover,  $\tan \delta$  peak values of PCL/H<sub>2</sub>O-PU-01 and PCL/H<sub>2</sub>O-PU-02 are higher than those of PCL/H<sub>2</sub>O-PU-03 and PCL/H<sub>2</sub>O-PU-04; these data indicate that PCL/H<sub>2</sub>O-PU-04 is the most viscous compound. From DMA,  $T_g$  of PCL/H<sub>2</sub>O-PU-01, PCL/H<sub>2</sub>O-PU-02, PCL/H<sub>2</sub>O-PU-03, and PCL/H<sub>2</sub>O-PU-04 is -35.1, -33.7, -30, and -29 °C, respectively (Table 2). The  $T_g$  value slightly increases with the H<sub>2</sub>O content; hence, the H<sub>2</sub>O or the hard-segment content enhances the dynamic mechanical properties.

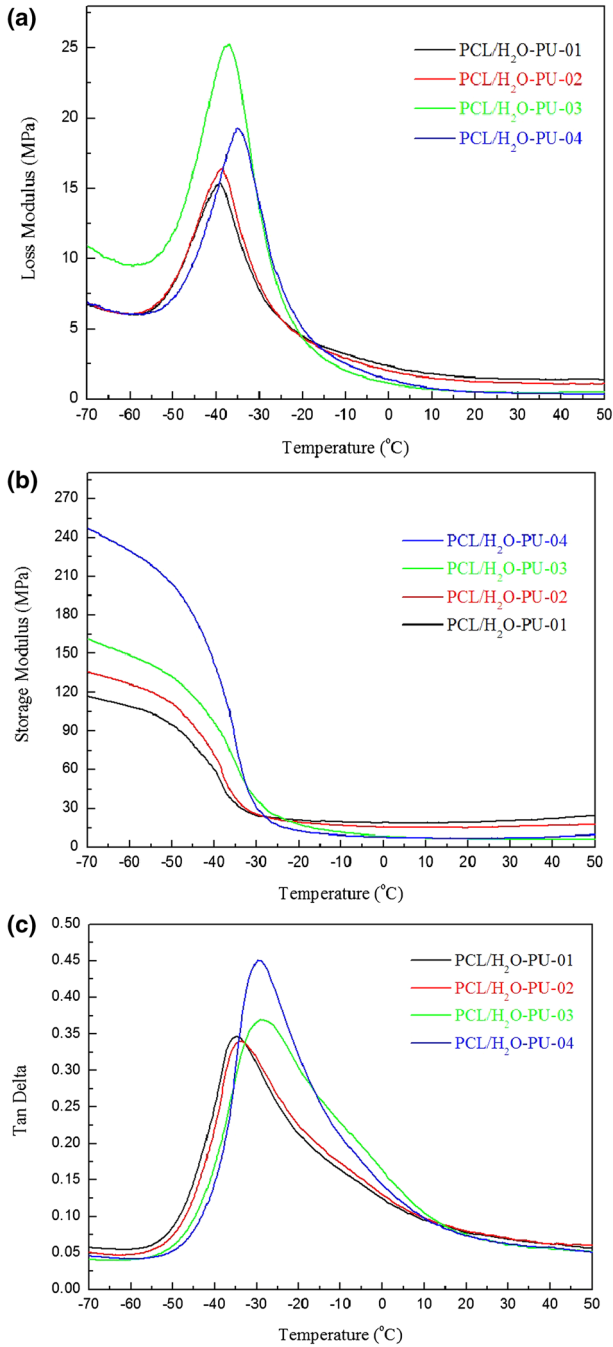


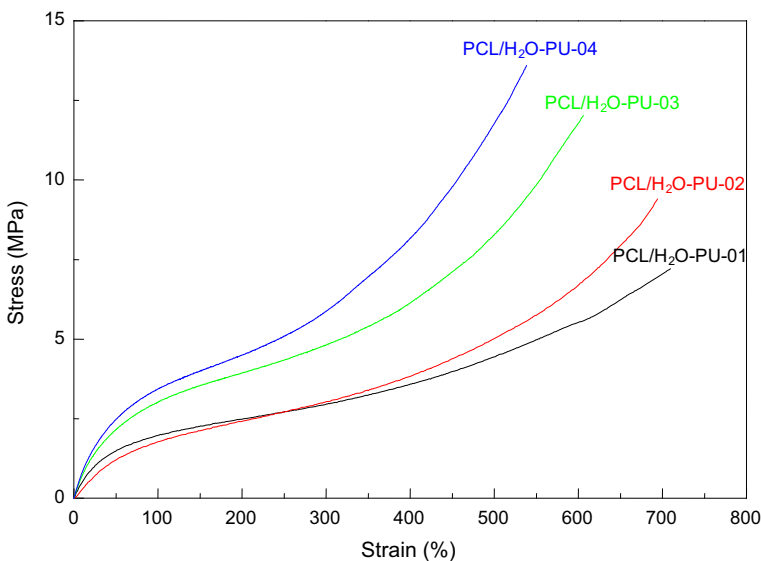
**Fig. 4** **a** Loss modulus, **b** storage modulus, and **c**  $\tan \delta$  curves of PCL/H<sub>2</sub>O-PU

## Tensile properties

Figure 5 plots the stress–strain curves for PCL/H<sub>2</sub>O-PU. The tensile strength of PCL/H<sub>2</sub>O-PU-01, PCL/H<sub>2</sub>O-PU-02, PCL/H<sub>2</sub>O-PU-03, and PCL/H<sub>2</sub>O-PU-04 is 7.2, 9.4, 12, and 13.6 MPa, respectively; the corresponding Young's modulus is 2.9, 3.1, 3.9, and 4.5 MPa; and the corresponding elongation at break is 709.6, 694.2, 606.2, and 538.5 %. With increasing H<sub>2</sub>O or hard-segment content, both the tensile strength and the Young's modulus increase. However, the elongation at break decreases. It is consistent with this behavior: storage module data indicate that the elasticity of PCL/H<sub>2</sub>O-PU decreases with increasing H<sub>2</sub>O at room temperature. The explanation is given as follows: as the hard-segment content increases, the micro-phase separation also increases [22].

## Gel permeation chromatography (GPC)

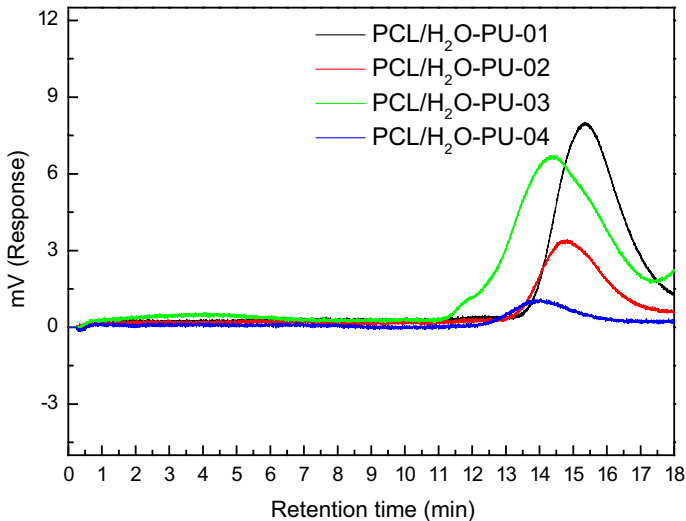
GPC data are summarized in Table 3. GPC was used to determine the number average molecular weight ( $M_n$ ), weight average molecular weight ( $M_w$ ), and molecular weight distribution ( $M_w/M_n$ ).  $M_n$  and  $M_w$  of PCL/H<sub>2</sub>O-PU are higher with increasing H<sub>2</sub>O content; it was anticipated that repeatable units of polymer are more in number as H<sub>2</sub>O increases during the synthesis. Moreover, the GPC analysis shows that the retention time is shorter as the H<sub>2</sub>O content increases. Figure 6 indicates that PCL/H<sub>2</sub>O-PU-01 elutes at 14.81 min. As the amount of H<sub>2</sub>O increases, larger molecules elute earlier than 14.81 min (from 14.27 to 1.46 min).



**Fig. 5** Tensile properties of PCL/H<sub>2</sub>O-PU

**Table 3** GPC for PCL/H<sub>2</sub>O-PU

	Retention time (min)	$\overline{M}_n$ ( $\times 10^4$ )	$\overline{M}_w$ ( $\times 10^4$ )	$\overline{M}_w/\overline{M}_n$
PCL/H <sub>2</sub> O-PU-01	14.81	1.55	2.55	1.6
PCL/H <sub>2</sub> O-PU-02	14.27	2.55	3.94	1.5
PCL/H <sub>2</sub> O-PU-03	13.84	3.60	8.05	2.3
PCL/H <sub>2</sub> O-PU-04	13.46	5.06	8.76	1.7

**Fig. 6** GPC chromatograms of PCL/H<sub>2</sub>O-PU

## Crytallinity

Figure 7 compares the XRD patterns of different compounds of PCL/H<sub>2</sub>O-PU; the patterns show no sharp or narrow diffraction halos. For each compound, two broad diffraction halos occur at  $2\theta = 21^\circ$  and  $10^\circ$ ; the one at  $10^\circ$  has a low intensity, and the other at  $21^\circ$  has a high intensity. The high-intensity values are 2047, 2183, 2206, and 2248 for PCL/H<sub>2</sub>O-PU-01, PCL/H<sub>2</sub>O-PU-02, PCL/H<sub>2</sub>O-PU-03, and PCL/H<sub>2</sub>O-PU-04, respectively. The compounds have a similar morphology because each diffraction halo corresponds to the same  $2\theta$  value. The diffraction halos are associated with the amorphous phase of PU. The diffraction halo with a high intensity tends to be narrow, which is associated with a crystalline phase. But the molecular weight of PCL is 530 g/mol, which is too low to exhibit a crystalline morphology; hence, only an amorphous phase was formed. The polymer chains in the amorphous phase of PCL/H<sub>2</sub>O-PU-04 can be relatively arranged because of its higher H<sub>2</sub>O or hard-segment content. However, this orderly arrangement of the polymer chains is still insufficient to attain the extent of crystalline or quasi-crystalline morphology.

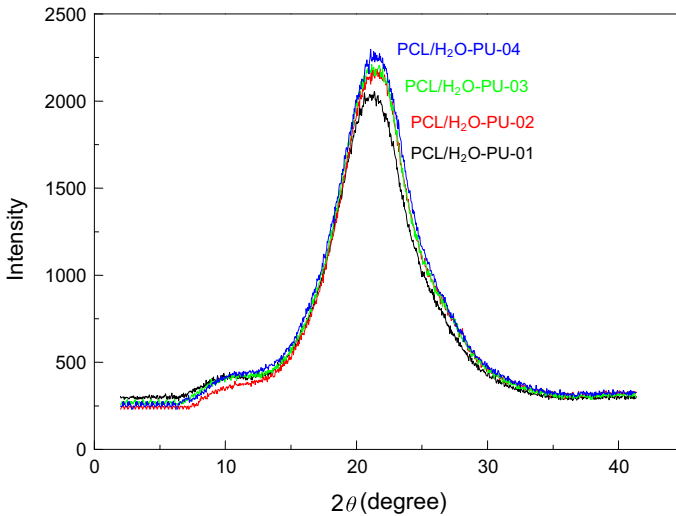


**Fig. 7** X-ray diffraction patterns of PCL/H<sub>2</sub>O-PU

### Swelling degree and hydrolytic degradation

PCL/H<sub>2</sub>O-PU-01, PCL/H<sub>2</sub>O-PU-02, PCL/H<sub>2</sub>O-PU-03, and PCL/H<sub>2</sub>O-PU-04 were immersed in a 20 wt% aqueous ethanol solution for 24 h; the swelling degree of each compound is 47.7, 46.8, 46.6, and 45.9 %, respectively (Table 1). The degree of swelling increases with the PCL content or decreases with increasing hard-segment content. There may be two factors that affect this swelling behavior: one is the hydrolytic degradable nature of PCL, and the other the physical cross-linking effect of the hard-segment. The higher the amount of PCL in the compound, the higher is the swelling degree. The presence of the hard-segment acts as a physical cross-link in polyurethane and subsequently enhances its physical properties, such as mechanical strength, hardness, and solvent resistance.

Hydrolytic degradation data for PCL/H<sub>2</sub>O-PU are analyzed (Fig. 8). PCL/H<sub>2</sub>O-PU-01 has the highest PCL content, and PCL/H<sub>2</sub>O-PU-04 has the lowest. The weight loss of a specimen after the hydrolytic degradation test increases with the test time and the PCL content. PCL is hydrolytically degradable; therefore, the specimen with a higher PCL content exhibits higher degradation. Water molecules easily diffuse into the weak regions; in other words, hydrolytic degradation occurs preferentially in soft-segment regions. Therefore, hydrolysis becomes more difficult when the hard-segment content is higher. For PCL/H<sub>2</sub>O-PU-01, maximum weight loss was attained after 18 days; it was 4.9 % at 37 °C and 6.85 % at 45 °C. Hence, degradation rates are also influenced by temperature; the higher the temperature, the faster is the hydrolytic degradation rate. This behavior is attributed to the greater expansion of the specimen volume at higher temperature; therefore, water molecules diffuse with greater ease into the specimen. Moreover, water molecules move more strongly at higher temperature and can easily disrupt the material.

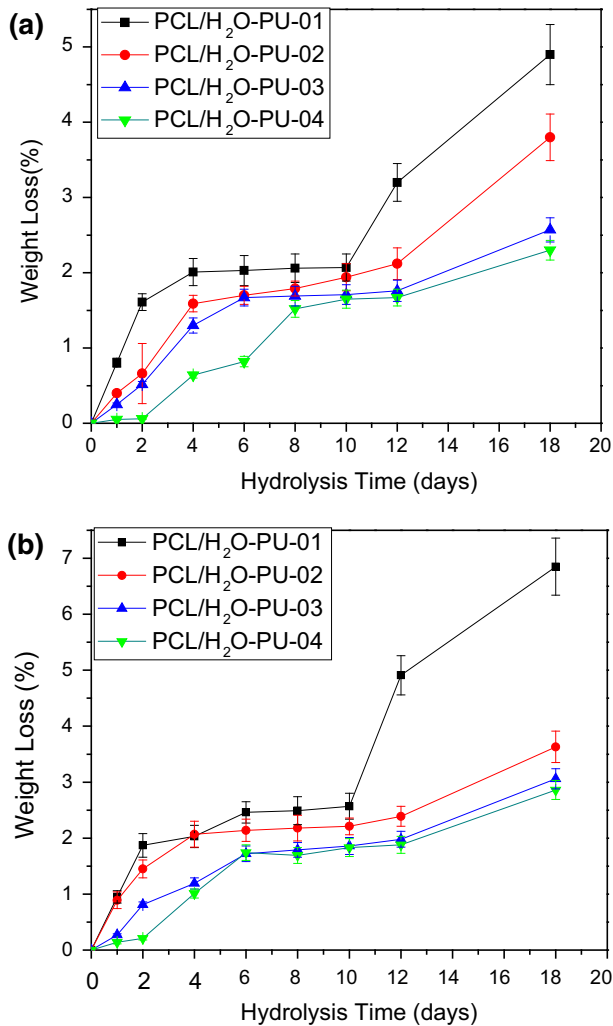


**Fig. 8** Hydrolytic degradation data for PCL/H<sub>2</sub>O-PU at (a) 37 and (b) 45 °C. *Error bars* are based on standard deviation for three replicated measurements

## Morphology

Figure 9 shows SEM micrographs of different compounds of PCL/H<sub>2</sub>O-PU before and after hydrolytic degradation. Before the degradation, the four compounds (Fig. 9a–d) show a wrinkled surface. The extruded wrinkle may represent the hard segment-rich phase. Compared with the soft-segment, the hard-segment with hydrogen bonding is less soluble in the NaOH solution. During the film formation process, the solvent is easily expelled from the vicinity of the hard-segment, so the hard-segment-rich phase aggregates and protrudes as wrinkles. The hard-segment

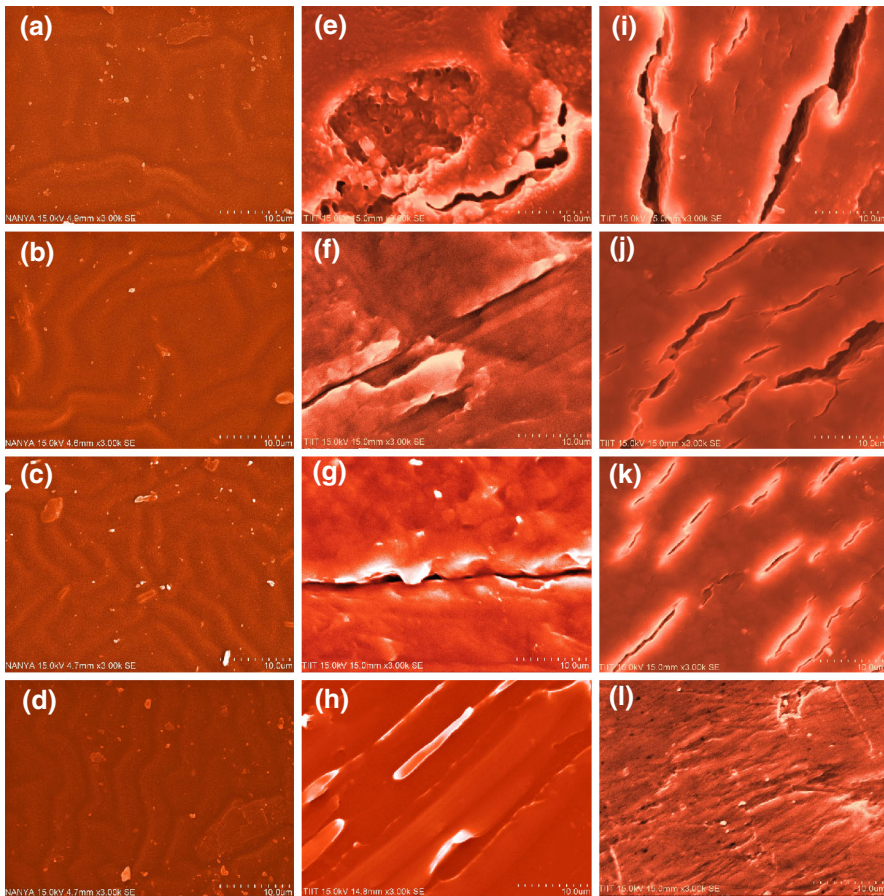


**Fig. 9** SEM micrographs. *First column* without hydrolytic degradation, *second column* with hydrolytic degradation for 18 days at 37 °C, and *third column* with hydrolytic degradation for 18 days at 45 °C. *First row* PCL/H<sub>2</sub>O-PU-01, *second row* PCL/H<sub>2</sub>O-PU-02, *third row* PCL/H<sub>2</sub>O-PU-03, and *fourth row* PCL/H<sub>2</sub>O-PU-04

content of PCL/H<sub>2</sub>O-PU-01 is the lowest, so the amount of wrinkles is the least. The hard-segment content of PCL/H<sub>2</sub>O-PU-04 is the highest, so the hard segment-rich phases or wrinkles in PCL/H<sub>2</sub>O-PU-04 are more entangled and become less protruded. After the hydrolytic degradation for 9 days at 37 °C, the SEM images of the compounds are shown in Fig. 9e–h. During the degradation process, the polymer chains are broken, and they rearrange causing the wrinkles to disappear. Cracks appear on the PCL/H<sub>2</sub>O-PU-01 surface (Fig. 9e; fewer cracks are on the surface of PCL/H<sub>2</sub>O-PU-02, PCL/H<sub>2</sub>O-PU-03, and PCL/H<sub>2</sub>O-PU-04 (Fig. 9f–h). Because water molecules diffuse with difficulty into the hydrophobic hard-segment, the specimen with a higher hard-segment or a lower soft-segment content degrades less than that with a lower hard-segment or a higher soft-segment content (Fig. 8). The surface of PCL/H<sub>2</sub>O-PU-01 in Fig. 9i shows more, deeper cracks than that in

Fig. 9e; the degradation at 45 °C causes more cracks to appear compared with that at 37 °C. This result is attributed to both the greater expansion of the specimen volume and the higher diffusion rate of water at a higher temperature. The specimen with a higher PCL content has a higher degradation than that with a lower PCL content. Therefore, PCL is an excellent ingredient for the synthesis of degradable polyurethane.

## Conclusions

In this study, to prepare a new type of polyurethane, PCL/H<sub>2</sub>O-PU, the materials used were PCL, MDI, PTMG, and H<sub>2</sub>O. The soft-segment was PCL, a biodegradable and biocompatible material. Various compositions of PCL/H<sub>2</sub>O-PU were prepared by varying the PCL or the H<sub>2</sub>O content. With increasing H<sub>2</sub>O content, the elongation at break of PCL/H<sub>2</sub>O-PU decreased, but the following properties increased: thermal resistance, glass transition temperature, tensile strength, and Young's modulus. The number average molecular weight and weight average molecular weight increased with the H<sub>2</sub>O content. Although the morphology of PCL/PDM-PU is amorphous, the compound polymer chains could be in a more orderly form because of the higher H<sub>2</sub>O content. With increasing PCL content, the degree of swelling in an aqueous ethanol solution and the hydrolytic degradation rate also increased. Hydrolytic degradation caused cracks in PCL/H<sub>2</sub>O-PU films. In general, increasing the PCL content enhanced the biodegradation of PCL/H<sub>2</sub>O-PU, whereas increasing the H<sub>2</sub>O content improved the mechanical properties of PCL/H<sub>2</sub>O-PU.

**Acknowledgments** The authors express their appreciation to Everlight Chemical Industrial Corporation, Far Eastern New Century Corporation, Apex Nanotek Corporation, Grabio Greentech Corporation, Ching-Yung Trading Co. Ltd., Fabric King Textile Co. Ltd., the Ministry of Economic Affairs (100-EC-17-A-10-S1-186), and the National Science Council (NSC 102-2221-E-161-011, NSC 100-3113-E-033-001, and NSC 102-2221-E-003-065) for supporting this work.

## References

1. Ni H, Skaja AD, Soucek MD (2000) Acid-catalyzed moisture-curing polyurea/polysiloxane ceramer coatings. *Prog Org Coat* 40:175–184
2. Gardner G (1996) Moisture-curing polyurethanes. *J Prot Coat Linings* 13:81–100
3. Chattopadhyay DK, Prasad PSR, Sreedhar B, Raju KVS (2005) The phase mixing of moisture cured polyurethane-urea during cure. *Prog Org Coat* 54:296–304
4. Chattopadhyay DK, Sreedhar B, Raju KVS (2006) The phase mixing studies on moisture cured polyurethane-ureas during cure. *Polymer* 47:3814–3825
5. Yukihiro N, Sato A, Sato S, Mori H, Endo T (2007) Synthesis of novel moisture-curable polyurethanes end-capped with trialkoxysilane and their application to one-component adhesives. *J Polym Sci, Part A: Polym Chem* 45:2689–2704
6. Ren D, Frazier CE (2012) Wood/adhesive interactions and the phase morphology of moisture-cure polyurethane wood adhesives. *Int J Adhes Adhes* 34:55–61
7. Datta J (2008) Rohn M, Structure, thermal stability and mechanical properties of polyurethanes, based on glycolysate from polyurethane foam waste, prepared with use of 1,6-hexanediol as a glycol. *Polimery* 53(11–12):871–875

8. Datta J (2010) Synthesis and investigation of glycolysates and obtained polyurethane elastomers. *J Elastom Plast* 42(2):117–127
9. Datta J, Kacprzyk M (2008) Thermal analysis and static strength of polyurethanes obtained from glycolysates. *J Therm Anal Calorim* 93(3):753–757
10. Datta J, Janicka M (2007) Synthesis and properties of polyurethanes made of secondary raw materials. *Przemysł Chemiczny* 86(7):624–626
11. Modesti M, Lorenzetti A (2002) Flame retardancy of polyisocyanurate-polyurethane foams. Use of different charring agents. *Polym Degrad Stab* 78(2):341–347
12. Tsou CH, Suen MC, Yao WH, Yeh JT, Wu CS, Tsou CY, Chiu SH, Chen JC, Wang RY, Lin SM, Hung WS, De Guzman M, Hu CC, Lee K-R (2014) Preparation and characterization of bioplastic-based green renewable composites from tapioca with acetyl tributyl citrate as a plasticizer. *Materials* 7(8):5617–5632
13. Tsou CH, Hung WS, Chen JC, Huang CY, Wu CS, Chiu SH, Tsou CY, Chen JC, Chu CK, Hu CC et al (2014) New composition of maleic-anhydride-grafted poly(lactic acid), rice husk with methylenediphenyl diisocyanate. *Mater Sci Medžiagotyra* 20(4):446–451.14
14. Tsou CH, Kao BJ, Suen MC et al (2014) Crystallization behavior and biocompatibility of poly (butylene succinate)/poly(lactic acid) composites. *Mater Res Innov* 18:372
15. Hatakeyama T, Izuta Y, Hirose S, Hatakeyama H (2002) Phase transitions of lignin based polycaprolactones and their polyurethane derivatives. *Polymer* 43:1177e82
16. Wang W, Ping P, Chen X, Jing X (2006) Polylactide-based polyurethane and its shape-memory behavior. *Eur Polym J* 42:1240–1249
17. Lee SI, Yu SC, Lee YS (2001) Degradable polyurethanes containing poly(butylene succinate) and poly(ethylene glycol). *Polym Degrad Stab* 72:1–87
18. Guan J, Sacks MS, Beckman EJ, Wagner WR (2004) Biodegradable poly(ether ester urethane)urea elastomers based on poly(ether ester) triblock copolymers and putrescine: synthesis, characterization and cytocompatibility. *Biomaterials* 25:85–96
19. Moore T, Adhikari R, Gunatillake P (2005) Chemosynthesis of bioresorbable poly(g-butylolactone) by ring-opening polymerisation: a review. *Biomaterials* 26:3771–3782
20. Yeganeh H, Jamshidi H, Jamshidi S (2007) Synthesis and properties of novel biodegradable poly( $\epsilon$ -caprolactone)/poly(ethylene glycol)-based polyurethane elastomers. *Polym Int* 56:41–49
21. Heijkants GJC, Calck RV, Tienen TG, Groot JH, Buma P, Pennings AJ, Veth PH, Schouten AJ (2005) Uncatalyzed synthesis, thermal and mechanical properties of polyurethanes based on poly( $\epsilon$ -caprolactone) and 1,4-butane diisocyanate with uniform hard segment. *Biomaterials* 26:4219–4228
22. Woo GLY, Mittelman MW, Santerre JP (2000) Synthesis and characterization of a novel biodegradable antimicrobial polymer. *Biomaterials* 21:1235–1246
23. Hatakeyama T, Izuta Y, Hirose S, Hatakeyama H (2002) Phase transitions of lignin-based polycaprolactones and their polyurethane derivatives. *Polymer* 43:1177–1182
24. Lamba NMK, Woodhouse KA, Cooper SL (1998) Polyurethanes in biomedical applications. CRC Press, Boca Raton
25. Sarkar D, Yang JC, Lopina ST (2008) Polymer/carbon nanotube nanocomposites via noncovalent grafting with end-functionalized polymers. *J Appl Polym Sci* 108:2345–2351
26. Sarkar D, Yang JC, Gupta AS, Lopina ST (2009) Synthesis and characterization of L-tyrosine based polyurethanes for biomaterial applications. *J Biomed Mater Res A* 90(1):263–271
27. Shah PN, Manthe RL, Lopina ST (2009) Electrospinning of L-tyrosine polyurethanes for potential biomedical applications. *Polymer* 50:2281–2289
28. Shah PN, Yun YH (2012) Cellular interactions with biodegradable polyurethanes formulated from L-tyrosine. *J Bio Appl* 0:1–15
29. Tsou CH, Lee HT, Tsai HA, Cheng HJ, Suen MC (2013) Synthesis and properties of biodegradable polycaprolactone/polyurethanes by using 2,6-pyridinedimethanol as a chain extender. *Polym Degrad Stab* 98:643–650
30. Lee HT, Tsou CH, Jou CH, Huang FC, Wang ML, Suen MC (2014) The effects of silver nitrate on the structure and properties of polyurethanes containing pyridyl units. *Polym Bull* 71:2749–2767